Analytical modeling of the interaction of an ultrasonic wave with a rough bone-implant interface

Yoann Hériveaux, Vu-Hieu Nguyen, Shiro Biwa, Guillaume Haiat

▶ **To cite this version:**

Yoann Hériveaux, Vu-Hieu Nguyen, Shiro Biwa, Guillaume Haiat. Analytical modeling of the interaction of an ultrasonic wave with a rough bone-implant interface. Ultrasonics, 2020, pp.106223. 10.1016/j.ultras.2020.106223 . hal-02911708

HAL Id: hal-02911708
https://hal.science/hal-02911708

Submitted on 9 Nov 2020

HAL is a multi-disciplinary open access archive for the deposit and dissemination of scientific research documents, whether they are published or not. The documents may come from teaching and research institutions in France or abroad, or from public or private research centers.

L'archive ouverte pluridisciplinaire **HAL**, est destinée au dépôt et à la diffusion de documents scientifiques de niveau recherche, publiés ou non, émanant des établissements d'enseignement et de recherche français ou étrangers, des laboratoires publics ou privés.

Analytical modeling of the interaction of an ultrasonic wave with a rough bone-implant interface

Yoann Hériveaux[a], Vu-Hieu Nguyen[b], Shiro Biwa[c], Guillaume Haïat[a]

[a] *CNRS, Laboratoire Modélisation et Simulation Multi Echelle, MSME UMR 8208 CNRS, 94010 Créteil Cedex, France*

[b] *Université Paris-Est, Laboratoire Modélisation et Simulation Multi Echelle, MSME UMR 8208 CNRS, 94010 Créteil Cedex, France*

[c] *Department of Aeronautics and Astronautics, Graduate School of Engineering, Kyoto University, Katsura, Nishikyo-ku, Kyoto 615-8540, Japan.*

Abstract

Quantitative ultrasound can be used to characterize the evolution of the bone-implant interface (BII), which is a complex system due to the implant surface roughness and to partial contact between bone and the implant. The determination of the constitutive law of the BII would be of interest in the context of implant acoustical modeling in order to take into account the imperfect characteristics of the BII. The aim of the present study is to propose an analytical effective model describing the interaction between an ultrasonic wave and a rough BII.

To do so, a spring model was considered to determine the equivalent stiffness K of the BII. The stiffness contributions related (i) to the partial contact between the bone and the implant and (ii) to the presence of soft tissues at the BII during the process of osseointegration were assessed independently. K was found to be comprised between 10^{13} and 10^{17} N/m^3 depending on the roughness and osseointegration of the BII. Analytical values of reflection and transmission coefficients at the BII were derived from values of K. A good agreement with numerical results obtained through finite element simulation was obtained. This model may be used for future finite element bone-implant models to replace the BII conditions.

Keywords: Bone-implant interface, Roughness, Osseointegration, Spring model, Finite element modeling.

1. Introduction

Endosseous cementless titanium implants have been used in orthopedic, dental and maxillofacial surgeries for more than 40 years, and have allowed considerable progresses to restore joints functionality and to replace missing teeth. However, despite a routine clinical use, osseointegration failures still occur and may have dramatic consequences. The implant surgical success is determined by the evolution of the implant stability [27], which is directly related to the biomechanical properties of the bone-implant interface (BII) [10, 13]. The biological tissues surrounding an implant are initially non-mineralized and may thus be described as soft tissues [31]. During normal osseointegration processes, periprosthetic bone tissue is progressively transformed into mineralized bone. However, in cases associated to implant failures, the aforementioned osseointegration phenomena do not occur in an appropriate manner, leading to the presence of fibrous tissues around

the implant and to the implant aseptic loosening, which is one of the major causes of surgical failure [37].

Different biomechanical techniques such as impact methods [41, 30, 44] or resonance frequency analysis [29, 33] have been applied to assess implant stability. Quantitative ultrasound (QUS) methods have the advantage of providing a better resolution compared to approaches using acoustic waves with a lower frequency range. The principle of QUS measurements lies on the dependence of the ultrasonic propagation at the BII on the bone-implant contact ratio (BIC) and on the bone mechanical properties. A combined increase of the BIC and of the periprosthetic bone Young's modulus [45] and mass density [26, 48] occurs during healing. All the aforementioned bone changes lead to a decrease of the reflection coefficient at the BII due to a decrease of the gap of acoustical properties, which has been evidenced experimentally [28]. Based on these results and on a preliminary study [1], a 10 MHz QUS device has been developed by our group to assess dental implant stability. It was validated first *ex vivo* using cylindrical implants [24], then *in vitro* using dental implants inserted in a biomaterial [46] and in bone tissue [47], and eventually *in vivo* [53]. Moreover, the sensitivity of QUS on the biomechanical properties of the BII was shown to be significantly higher compared to resonance frequency analysis *in vitro* [52] and *in vivo* [51].

The various parameters influencing the interaction between an ultrasonic wave and the BII are difficult to control when following an experimental approach and are likely to vary in parallel. Therefore, acoustical modeling and numerical simulation are useful in order to precisely estimate the effects of the mechanical and geometrical properties of the implant and of bone tissue.

Ultrasonic propagation has been simulated in cylindrical implants [25] and in dental implants [49, 50, 39] using 2-D finite difference time domain and 3-D finite element models (FEM). However, the aforementioned studies considered a fully-bonded BII and did not account for the combined effect of the surface roughness and bone growth around the implant. Since osseointegration was only modeled through variations of the biomechanical properties of periprosthetic bone tissue, the influence of the BIC ratio could not be considered either. More recently, a 2-D FEM has been developed to investigate the sensitivity of the ultrasonic response to multiscale surface roughness properties of the BII and to osseointegration processes [18, 17, 19]. The implant roughness was modeled by a sinusoidal profile and the thickness of a soft tissue layer comprised between the bone and the implant was progressively reduced to simulate osseointegration phenomena. The sinusoidal description of the surface profile was shown to be adapted (i) at the macroscopic scale because it mimicks implant threading and (ii) at the microscopic scale since equivalence between the ultrasonic response of sinusoidal profiles and of real implant profiles measured by profilometry was established [17]. Moreover, 2-D modeling was shown to be sufficient to describe the ultrasonic propagation at the BII [19]. However, only numerical approaches have been developed to model the propagation of QUS at the BII. Analytical modeling could be of interest in order to determine the constitutive law corresponding to the interaction between an ultrasonic wave and an osseointegrating BII, which could then be used to replace the BII conditions in future FEM of bone-implant systems.

Different approaches have been developed to simulate the interaction of an elastic wave with rough interfaces, especially in the context of non-destructive testing and for geological applications. In particular, Baik and Thompson [3] developed a quasi-static model studying the ultrasonic scattering from imperfect interfaces. Lekesiz et al. [23] assessed the effective spring stiffness of a periodic array of collinear cracks at an interface between two dissimilar materials. The geometric configuration of this model may be of interest to describe a BII, but it cannot take into account the presence of soft tissues at the BII. Pecorari and Poznic [36] experimentally investigated the

effect of a fluid layer confined between two solid rough surfaces on the acoustic non-linear response of an interface, and highlighted that none of the current models from the literature could give an accurate description of the acoustical behavior of liquid-confining interfaces. More recently, Dwyer-Joyce et al. [7] separately assessed the solid contact stiffness and the fluid stiffness and then added these two contributions in order to describe the ultrasonic propagation near elastohydrodynamic lubricated contacts. However, to the best of our knowledge, such methods have never been applied in the literature to model the BII. The use of spring models to describe a BII has been introduced by Egan and Marsden [8] to describe load transfers at the BII and was more recently considered by [38], but none of these studies investigated the acoustical behavior of the BII.

The aim of the present work is to derive an analytical model describing the propagation of an ultrasonic wave at the BII. To do so, a spring model was considered. Two springs acting in parallel were introduced between the bone and the implant, as illustrated in Figure 1b. The first spring represents the contribution K_c of the contact between the bone and the implant, while the second spring represents the contribution K_{st} due to the presence of soft tissues at the interface. The equivalent stiffness K of the BII was determined analytically by separately assessing K_c and K_{st}. Analytical values of the reflection and transmission coefficients were derived from the stiffness values. Analytical values of the stiffness and of the reflection and transmission coefficients of the BII were compared with numerical results, which were determined using the FEM previously developed in Heriveaux et al. [18].

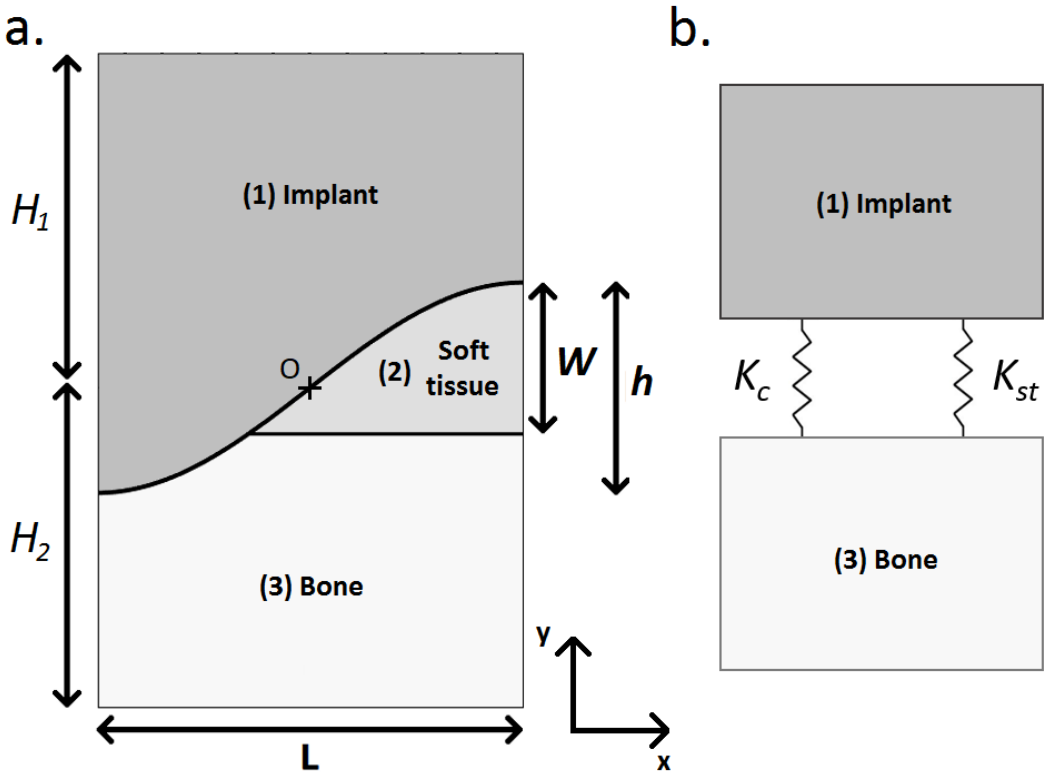

Figure 1: Schematic illustrations of (a) the 2-D numerical model and of (b) the analytical spring model.

2. Material and methods

2.1. General strategy

In previous studies [18, 17], a numerical model describing the propagation of an ultrasonic wave at the BII was developed. Based on this model, the reflection and transmission coefficients (r, t) at the BII can be assessed numerically, which will be recalled in Section 2.2.2. In the present work, an analytical model is proposed (see Section 2.3) in order to assess the values of the reflection and transmission coefficients (r, t).

The general strategy used herein (i) to develop the analytical model and (ii) to compare analytical results with their numerical counterparts is illustrated in Fig. 2 and will be described in what follows. Note that the superscript *num* refers to numerical results, while the superscript *ana* refers to analytical results.

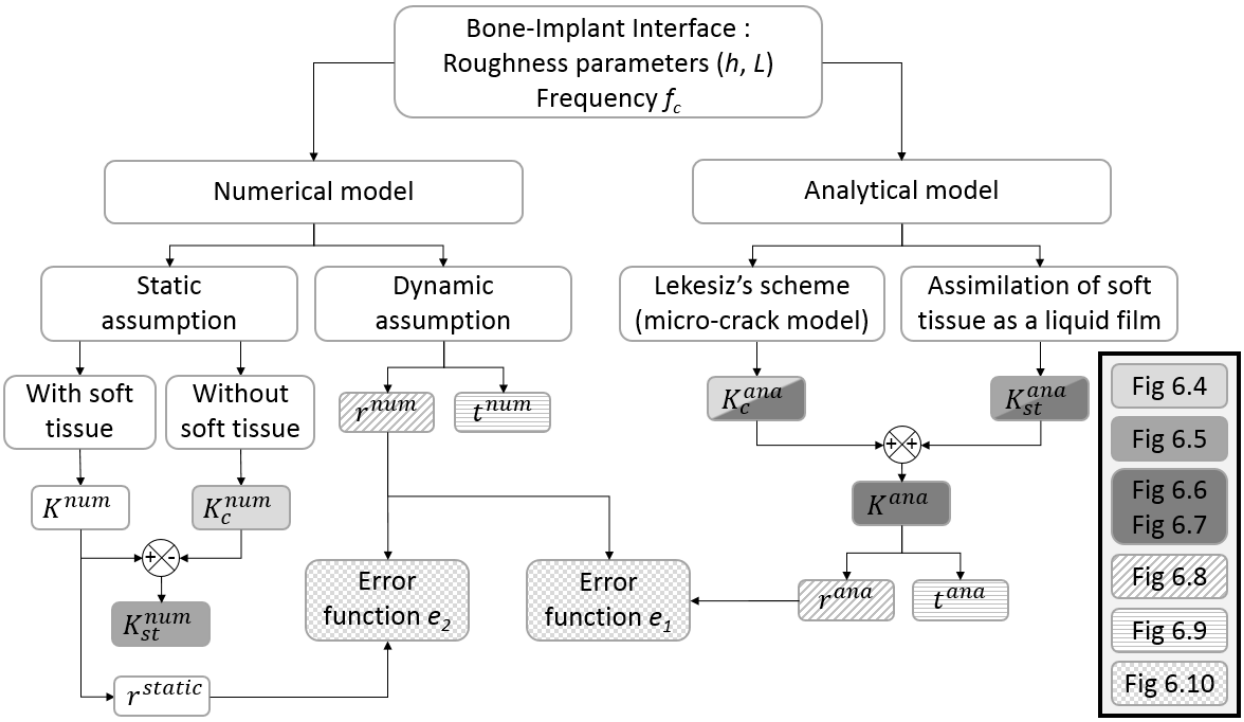

Figure 2: Schematic description of the numerical and analytical models developed to describe the interaction between the BII and an ultrasonic wave. The parameters plotted in Figures 4, 5, 6, 7, 8, 9 and 10 are represented with different fonts.

2.2. Numerical model

The numerical model considered herein was adapted from Heriveaux et al. [18, 17], Raffa et al. [38]. Two different studies were carried out with this model. First, the values of reflection and transmission coefficients (r^{num}, t^{num}) of the BII were retrieved through a numerical study carried out in the time domain. Second, the equivalent stiffness K^{num} of the BII was estimated through a static study. Both studies considered the same geometry for the BII, which will be described in what follows:

2.2.1. Description of the geometry of the model

As illustrated in Fig. 1, two coupled 2-dimensional half-spaces were separated from each other by an interphase. The first domain corresponds to the implant made of titanium alloy (Ti-6Al-4V, noted (1) in Fig. 1) and the other one represents bone tissue (noted (3) in Fig. 1). The implant surface profile was defined by a sinusoidal function of amplitude h and half-period L through the following expression:

$$y = \frac{h}{2} sin\left(\frac{\pi x}{L}\right) \tag{1}$$

Only a single half-sine period of the interface was considered, which is sufficient to simulate the propagation of the acoustic wave using symmetrical boundary conditions for the interfaces perpendicular to the direction x. The point of origin of the model was defined as the middle of the half-sine and is noted O in Fig 1a.

A soft tissue layer was considered between the bone and the implant (noted (2) in Fig. 1a) in order to model non-mineralized fibrous tissue that may be present at the BII just after surgery or in the case of non-osseointegrated implants [16]. The thickness W of the soft tissue layer was defined by the distance between the highest point of the sinusoidal surface profile and the bone level, as shown in Fig. 1a. The process of osseointegration was associated to a decrease of the value of W from $2h$ down to 0.

The total lengths of the implant and of the bone domain, denoted H_1 and H_2 respectively, were chosen to be able to distinguish the signal reflected from the interface and to avoid any reflection from the boundary of the simulation domain. Namely a value of $H_1 = H_2 = 10$ cm was chosen throughout the study.

All media were assumed to have homogeneous isotropic mechanical properties. The values used for the different media are shown in Table 1 and were taken from [32, 35, 34, 15].

Table 1: Material properties used in the numerical simulations.

	C_p (m.s^{-1})	C_s (m.s^{-1})	ρ (kg.m^{-3})
Soft tissues	1500	10	1000
Titanium	5810	3115	4420
Cortical bone tissue	4000	1800	1850

Different boundary conditions have been considered for the dynamic and static studies. For the dynamic study, a uniform pressure $p(t)$ was imposed at the top boundary of the implant domain (at $y = H_1$, see Fig. 1a). For the static study, a uniform constant tensile stress $\sigma = 1$ MPa was imposed at the top boundary of the implant domain (at $y = H_1$). For both studies, a fixed boundary was imposed at the bottom of the bone domain (at $y = -H_2$), which is supposed to be sufficiently large so that reflected waves on the bottom boundary of the model may be neglected.

2.2.2. Dynamic study

Time-dependent simulations were performed in order to determine the reflection and transmission coefficients (r_{num}, t_{num}) of the model. The governing equations have been described in details in Heriveaux et al. [18] and the reader is referred to this publication for further details. Briefly, the classical equations of elastodynamic wave propagation in isotropic solids were considered. The

continuity of the displacement and of the traction vector fields were considered at each interface (i - j), where {i,j} = {1,2}, {1,3} or {2,3}. The symmetric boundary conditions also impose that $u_x = 0$ at the lateral surfaces (x = -$L/2$ and $x = L/2$).

The acoustical source was modeled as a broadband ultrasonic pulse with a uniform pressure $p(t)$ applied at the top surface of the implant domain (see Fig. 1a) defined by:

$$p(t) = Ae^{-4(f_c t-1)^2} \sin(2\pi f_c t) \tag{2}$$

where A is an arbitrary constant (all computations are linear) representing the signal amplitude and f_c is its central frequency, which may vary between 2 and 15 MHz in the present study.

The system of dynamic equations was solved in the time domain using a finite element software (COMSOL Multiphysics, Stockholm, Sweden). The implicit direct time integration generalized-α scheme [5] was used to calculate the transient solution. The elements size was chosen equal to $\lambda_{min}/10$, where λ_{min} corresponds to the shortest wavelength in the simulation subdomain. The implant and bone subdomains were meshed by structured quadrangular quadratic elements and the soft tissues subdomain was meshed with triangular quadratic elements. The time step was chosen using the stability Courant-Friedrichs-Lewy (CFL) condition $\Delta t \leq \alpha \min(h_e/c)$ where $\alpha = 1/\sqrt{2}$, h_e is the elements size and c is the velocity in the considered subdomain. For simulations presented here, the time step is set at $\Delta t = 4 \times 10^{-3}/f_c$ (s).

The reflection and transmission coefficients were determined for each configuration. To determine the reflection coefficient, the signal representing the displacement along the direction of propagation was averaged along an horizontal line located at $y = H_1/2$. Two signals were compared to determine the reflection coefficient r^{num}. The first signal corresponds to the averaged simulated incident signal, noted $s_i(t)$. The second signal corresponds to the averaged simulated reflected signal, noted $s_r(t)$. The moduli of the Hilbert's transform of $s_i(t)$ and $s_r(t)$ were computed, and the maximum amplitudes of these envelopes are noted A_i and A_r, respectively. The reflection coefficient in amplitude is determined by:

$$r^{num} = A_r/A_i \tag{3}$$

Similarly, in order to determine the transmission coefficient, the signal representing the displacement along the direction of propagation was averaged along an horizontal line located at y = -$H_2/2$. The obtained signal corresponds to the averaged simulated transmitted signal, noted $s_t(t)$. The moduli of the Hilbert's transform of $s_t(t)$ was computed, and the maximum amplitudes of this envelope is noted A_t. The reflection coefficient in amplitude is determined by:

$$t^{num} = A_t/A_i \tag{4}$$

2.2.3. Static study

A static study was performed in order to determine the numerical stiffness K^{num} of the model. The approach used herein was similar to the one described in Raffa et al. [38]. The system of static equations was solved using the finite element software COMSOL Multiphysics, and domains were meshed in the same way as for the dynamic study. The total vertical displacement ΔH of the model due to the tensile stress σ was determined, and was related to the different parameters of

the model through the relation:

$$\Delta H = H_1 \frac{\sigma}{\lambda_{ti} + 2\mu_{ti}} + H_2 \frac{\sigma}{\lambda_b + 2\mu_b} + \frac{\sigma}{K^{num}}, \tag{5}$$

where (λ_{ti}, μ_{ti}) (respectively (λ_b, μ_b)) are the Lamé parameters of the titanium implant (respectively bone) corresponding to the values of (ρ, C_p, C_s) listed in Table 1. Therefore, the stiffness value of the interface K^{num} could be numerically assessed through the following expression:

$$K^{num} = \frac{1}{\frac{\Delta H}{\sigma} - \frac{H_1}{\lambda_{ti}+2\mu_{ti}} - \frac{H_2}{\lambda_b+2\mu_b}} \tag{6}$$

The relative stiffness contributions K_c^{num} due to the contact between the implant and the bone, and K_{st}^{num} due to the presence of the soft tissue layer between the implant and the bone were also determined numerically. In order to assess K_c^{num}, soft tissues were replaced by vacuum for the material (2) of the model (see Fig. 1a). Simulations were performed similarly as for the estimation of K^{num}, and K_c^{num} was estimated through Eq. 6. Note that K_c^{num} could only be estimated for $W < h$ since for $W > h$, there is no more contact between the bone and the implant. Therefore, in this latter case, K_c was considered equal to 0.

Finally, the contribution K_{st}^{num} was assessed through the relation :

$$K_{st}^{num} = K^{num} - K_c^{num} \tag{7}$$

2.3. Analytical model

A spring model was considered to assess the analytical value of the BII stiffness, as illustrated in Fig. 1b. First, the stiffness contribution K_c^{ana} due to the contact between implant and bone was assessed considering the model described in Lekesiz et al. [23]. Second, the stiffness contribution K_{st}^{ana} due to the presence of the soft tissue layer was assessed considering the work of Dwyer-Joyce et al. [7]. Finally, the total stiffness of the interface was defined by:

$$K^{ana} = K_c^{ana} + K_{st}^{ana} \tag{8}$$

2.3.1. Stiffness K_c^{ana} due to the bone-implant contact

The analytical expression of the stiffness due to the bone-implant contact K_c^{ana} was obtained from Lekesiz et al. [23]. Assuming that all materials are elastic, Lekesiz et al. [23] provide a closed-form analytical expression for the effective spring stiffness of an infinite array of micro-cracks of length $2a$ spaced at a constant interval $2b$ along the bond line between two dissimilar materials (see Fig. 3b), namely the implant and the bone in the present study. To do so, Lekesiz considered the framework of the open crack model [9], and took into account the effect of interactions between cracks. The expression of K_c^{ana} was determined as follows:

$$K_c^{ana} = \frac{G_{ti}}{b(3-4\nu_{ti})} \frac{(1+\alpha)}{(1-\beta^2)(1+4\epsilon^2)} \frac{\pi}{\ln\left(\sec(\frac{\pi a}{2b})\right)} \tag{9}$$

where (α, β) are the two Dundurs' parameters [6] depending on the mechanical properties of the bone and of the implant, $\epsilon = \frac{1}{2\pi} ln(\frac{1-\beta}{1+\beta})$ is the oscillation index, ν_{ti} is the Poisson's ratio of the titanium implant and G_{ti} is the shear modulus of the implant.

Figure 3a shows the sinusoidal BII considered in the numerical studies, and figure 3b shows the corresponding geometric configuration considered in Lekesiz et al. [23]. In order to derive an equivalence between both models, the soft tissues regions from the numerical model were assimilated to the interfacial cracks from the model of Lekesiz et al. [23]. This geometric approximation is only valid for $W < h$ since there is no more contact between the bone and the implant when $W > h$. Therefore, in this latter case, K_c^{ana} was considered equal to 0. Note that the validity of this approximation may decrease when the roughness amplitude h increases.

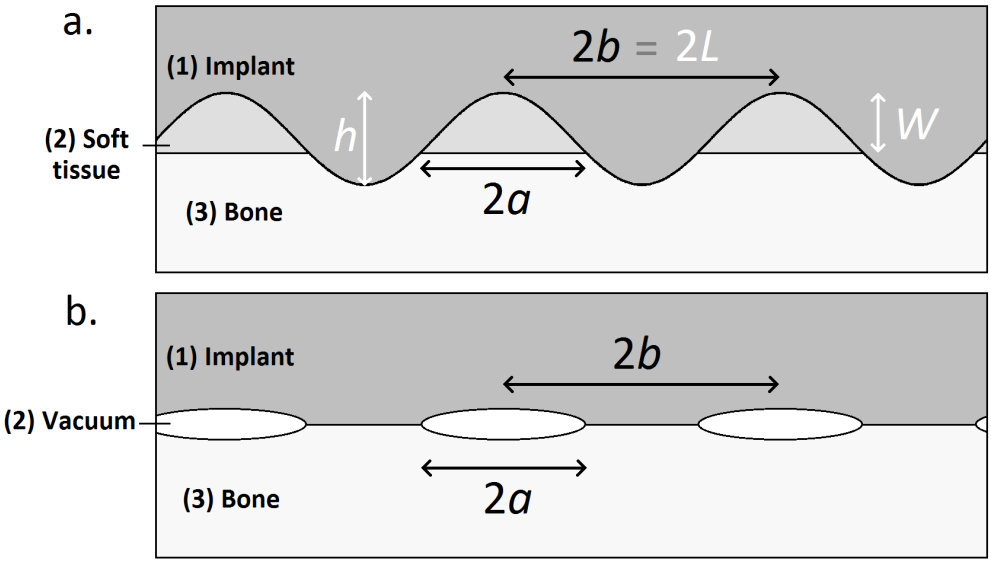

Figure 3: Geometric configurations of the interface considered (a) in the present work and (b) in Lekesiz et al. [23]. Parameters written in white represent the ones that were used in the numerical model (see Fig 1a) and parameters written in black correspond to the ones used in the work of Lekesiz et al. [23]

From this approximation, relations between the geometric parameters (a,b) from Lekesiz et al. [23] and (h, L, W) from the numerical model were obtained. First, the period of the sinusoidal roughness $2L$ corresponds to the periodicity of cracks $2b$ (see Fig. 3a), so that $b = L$. Second, the length of contact between the bone and soft tissues corresponds to the diameter of the cracks, *i.e.* to $2a$. Based on the sinusoidal expression of the implant roughness, a was defined as:

$$a = L\left(\frac{1}{2} - \frac{\arcsin\left(1 - \frac{2W}{h}\right)}{\pi}\right) \tag{10}$$

From the expressions of a and b, it may be noticed that K_c^{ana} depends on the geometrical parameters of the interface only through L and W/h.

2.3.2. Stiffness K_{st}^{ana} due to the presence of a soft tissue layer

Soft tissues have a low S-wave velocity C_s compared to their P-wave velocity C_p (see Table 1) and mechanical properties similar to those of liquid, so that they may be assimilated to a thick liquid film present between the bone and the implant. Therefore, the work of Dwyer-Joyce et al. [7] was considered to assess the analytical expression K_{st}^{ana} of the stiffness contribution due to the presence of soft tissues. Dwyer-Joyce et al. [7] studied the stiffness of a lubricated interface by first

considering a rough dry interfacial contact and then adding the contribution of the lubricant layer. The following expression was provided:

$$K_{st}^{ana} = \frac{\rho C_p^2}{d} \tag{11}$$

where ρ is the density of soft tissues, C_p is the P-wave velocity in soft tissues (see Table 1) and d is the gap thickness at the interface. In our case, d corresponds to the mean soft tissues thickness at the interface and was geometrically established through the following expression:

$$d = \begin{cases} \left(W - \frac{h}{2}\right)\left(\frac{1}{2} - \frac{\arcsin(1-\frac{2W}{h})}{\pi}\right) + \frac{\sqrt{hW-W^2}}{\pi}, & \text{if } W \leq h \\ W - \frac{h}{2}, & \text{if } W \geq h \end{cases} \tag{12}$$

In particular, the expression of d defined by Eq. 12 is continuous, with $d = h/2$ for $W = h$. Note that K_{st} could not be assessed analytically for $W = 0$ because there is no soft tissue at the BII in that configuration ($d = 0$). The total analytical stiffness K^{ana} of the BII was eventually defined following:

$$K^{ana} = K_c^{ana} + K_{st}^{ana} \tag{13}$$

2.4. Reflection and transmission coefficients

Based on a quasi-static approach in the frequency domain, Tattersall [42] derived the following expressions of the analytical reflection and transmission coefficients (r_f^{ana}, t_f^{ana}) corresponding to the interaction between an ultrasonic wave at an interface:

$$r_f^{ana} = \frac{Z_{ti} - Z_b + i\omega Z_{ti} Z_b / K^{ana}}{Z_{ti} + Z_b + i\omega Z_{ti} Z_b / K^{ana}} \tag{14}$$

$$t_f^{ana} = \frac{2Z_{ti}}{Z_{ti} + Z_b + i\omega Z_{ti} Z_b / K^{ana}} \tag{15}$$

where Z_{ti} and Z_b correspond to the acoustical impedance of titanium and of bone, respectively.

Since the numerical study was performed in the time domain, Eq. 14 and 15 were transformed into the time domain to determine (r^{ana}, t^{ana}) so that the analytical and numerical results could be compared. To do so, r_f^{ana} (respectively t_f^{ana}) was convoluted by the Laplace transform of the ultrasonic excitation pulse $p(t)$ (see Eq. 2). An inverse Laplace transform was then applied to obtain the analytical reflected signal s_r^{ana}(t) (respectively the analytical transmitted signal $s_t^{ana}(t)$). Similarly as for numerical signals (see Section 2.2.2), the moduli of the Hilbert's transform of $s_r^{ana}(t)$ and $s_t^{ana}(t)$ were computed, and the maximum amplitudes of these envelopes were retrieved to assess the analytical coefficients r^{ana} and t^{ana}.

In order to estimate the difference between the numerical and analytical models, an error function e_1 corresponding to the mean difference between the analytical and numerical reflection coefficients for 4 values of central frequencies f_c and 10 values of W/h was introduced:

$$e_1 = \sum_{i=1}^{4} \sum_{j=1}^{10} \frac{|r^{ana}(f_c(i), W/h(j)) - r^{num}(f_c(i), W/h(j))|}{40} \tag{16}$$

Note that in Eq. 16, r^{ana} and r^{num} were determined in the time domain for input signals of

frequency $f_c(i)$ ($i \in [1,4]$) and considering a ratio of W and h equal to $W/h(j)$ ($j \in [1,10]$).

Moreover, the reflection coefficient r^{static} derived from the numerical static study was also assessed by introducing the numerical values of K^{num} determined in Section 2.2.3 into Eq. 14 instead of K^{ana}, and compared to analytical results in order to validate the model presented here. Similarly as for analytical results, the difference between r^{num} and r^{static} was assessed through the error function e_2:

$$e_2 = \sum_{i=1}^{4} \sum_{j=1}^{10} \frac{|r^{static}(f_c(i), W/h(j)) - r^{num}(f_c(i), W/h(j))|}{40} \tag{17}$$

Table 2 shows all values of f_c and W/h that were used to estimate e_1 and e_2. In particular, ratios W/h were considered between 0 and 2 since it represents the main configuration of interest from a physiological point of view [53, 51]. Moreover, values of W/h equal to 0.99 and 1.01 were considered because $W/h = 1$ constitutes a critical situation where bone stops being in contact with the implant.

Table 2: Values of the parameters used to estimate the error functions e_1 and e_2, employed to compare the numerical and analytical results.

	Values considered
Ratio W/h	{0; 0.25; 0.5; 0.75; 0.99; 1.01; 1.25; 1.5; 1.75; 2}
Frequency f_c (MHz)	{2; 5; 10; 15}

3. Results

3.1. Stiffness K_c due to the bone-implant contact

Figure 4 presents the variation of the numerical and analytical contact interface stiffness K_c as a function of the ratio of the soft tissues thickness W and the roughness amplitude h for $L = 50$ µm. Different values of h were considered for K_c^{num}, while K_c^{ana} was shown to be independent from h for a given value of W/h. K_c decreases as a function of W/h, especially for values of W/h close to 0 and 1. In particular, K_c^{ana} tends towards infinity when W/h tends towards 0, and K_c^{ana} tends towards 0 when W/h tends towards 1. A relatively good agreement is obtained between K_c^{num} and K_c^{ana}. However, the difference between numerical and analytical results increases for higher values of h. Moreover, except for the case $W/h = 0$, K_c^{ana} always remains lower than K_c^{num}.

3.2. Stiffness K_{st} due to the presence of a soft tissue layer

Figure 5 shows the variation of the analytical and numerical stiffness K_{st} due to the presence of soft tissues as a function of the ratio of the soft tissues thickness W and the roughness amplitude h for $L = 50$ µm and for different values of h. K_{st} decreases as a function of W/h and as a function of h. A relatively good agreement is obtained between analytical and numerical values when $W/h > 1$. However, for lower values of W/h, K_{st}^{num} is significantly higher than K_{st}^{ana}, especially for high values of h.

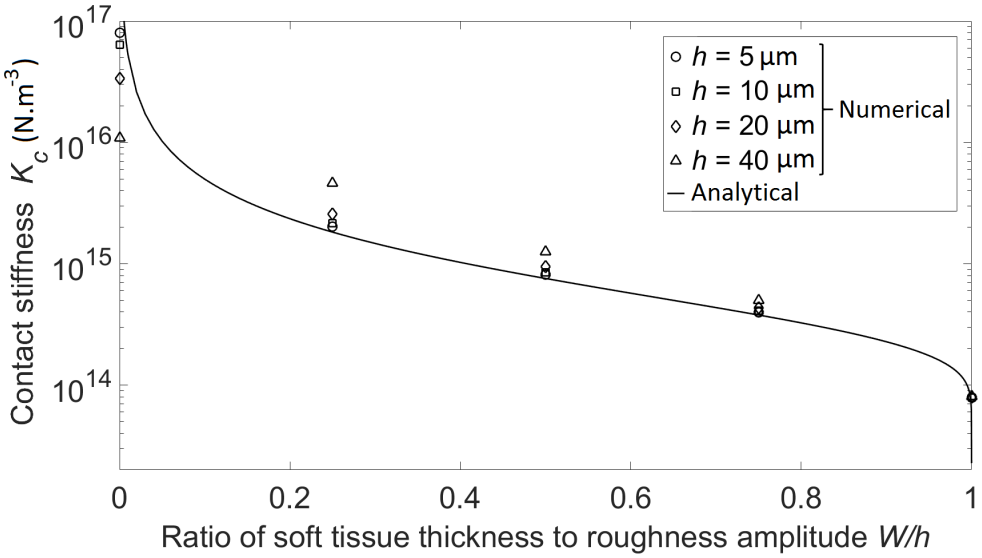

Figure 4: Variation of the contact interface stiffness K_c as a function of the ratio of the soft tissues thickness W and the roughness amplitude h for $L = 50$ µm. The solid line represents the analytical expression of K_c and punctual values represent values of stiffness obtained through numerical simulation for different values of h.

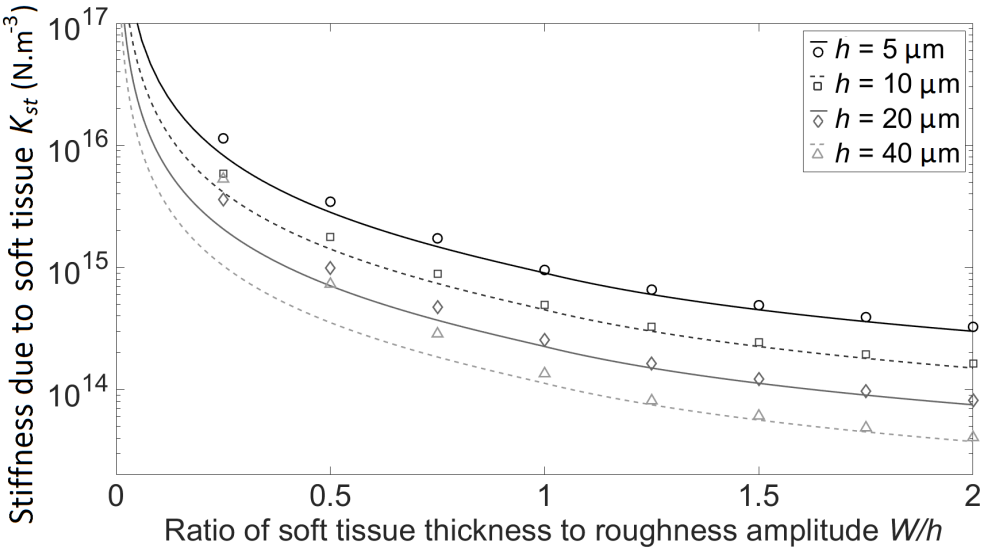

Figure 5: Variation of the interface stiffness due to the presence of a soft tissue layer K_{st} as a function of the ratio of the soft tissues thickness W and the roughness amplitude h for $L = 50$ µm and for different values of h. The solid lines represent the analytical expression of K_{st} and punctual values represent values of stiffness obtained through numerical simulation.

3.3. Total stiffness of the interface K

Figure 6 presents the evolution of K_c^{ana}, K_{st}^{ana} and K^{ana} as a function of the ratio the soft tissues thickness W and of the roughness amplitude h for $L = 50$ µm and for different values of h. For low values of h ($h = 5$ µm and $h = 10$ µm), the contribution of the contact stiffness is low compared to the contribution due to the presence of soft tissues. For $h = 20$ µm, both

contributions are in the same order of magnitude. For $h = 40$ µm, the contribution of the contact stiffness becomes higher to the one due to the presence of soft tissues. For all values of h, a steep decrease of K is obtained around $W/h = 1$, which corresponds to the point where the bone and the implant stops being in contact, so that K_c suddenly decreases to 0. Moreover, this decrease is more pronounced for higher values of h.

Figure 7 presents the evolution of K_c^{ana}, K_{st}^{ana} and K^{ana} as a function of the ratio the soft tissues thickness W and the roughness amplitude h for $h = 20$ µm and for different values of L. Figure 6 shows that for $L = 50$ µm, K_c and K_{st} are within the same range of values for $h = 20$ µm. Fig. 7 shows that for higher values of L ($L = 75$ µm and $L = 100$ µm), K_c is lower than K_{st}, while for lower values of L ($L = 40$ µm and $L = 25$ µm), K_c is higher than K_{st}.

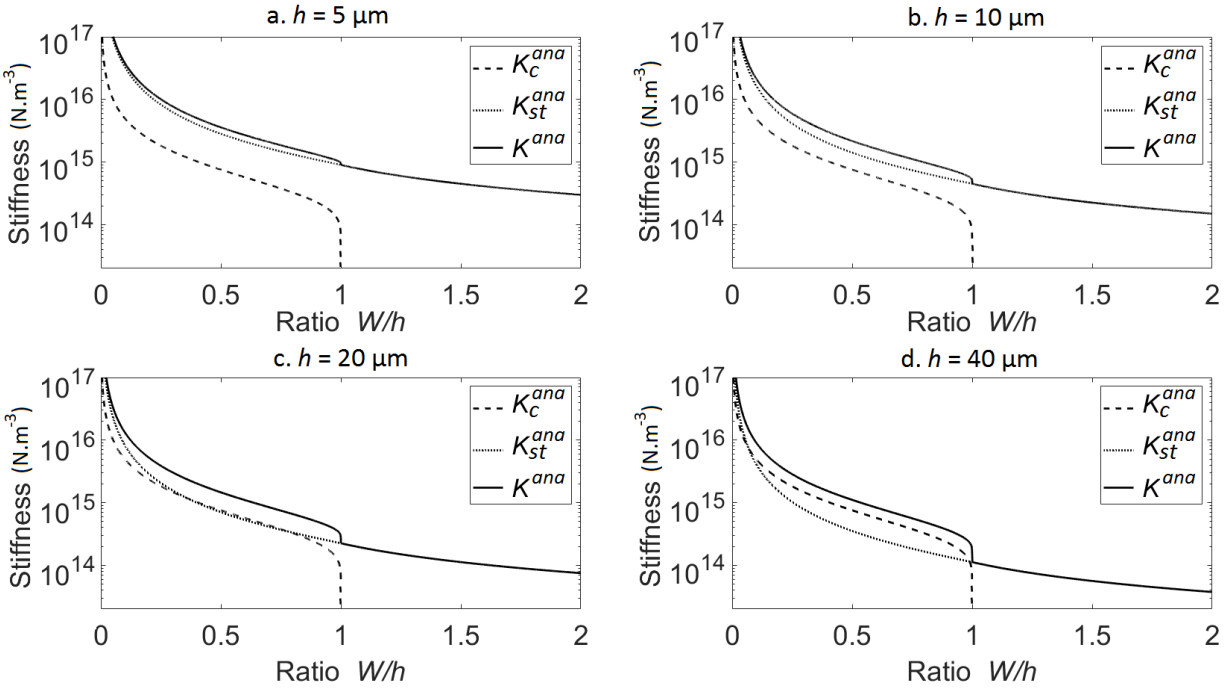

Figure 6: Variation of the analytical total stiffness of the BII K^{ana} and of the stiffness contributions K_c^{ana} and K_{st}^{ana} corresponding to the bone-implant contact and to soft tissues, respectively, as a function of the ratio of the soft tissues thickness W and the roughness amplitude h for $L = 50$ µm and (a) $h = 5$ µm, (b) $h = 10$ µm, (c) $h = 20$ μm, (d) $h = 40$ µm.

3.4. Comparison between analytical and numerical reflection and transmission coefficients

Figure 8 shows the variation of r^{num} and r^{ana} as a function of W/h for $L = 50$ μm and for different values of h. Figure 9 shows the variation of t^{num} and t^{ana} as a function of the ratio W/h for $L = 50$ μm and for different values of h. The reflection coefficient increases as a function of W/h and of f_c, while the transmission coefficient decreases as a function of W/h and of f_c.

Overall, a good agreement is obtained between analytical and numerical results. In particular, a steep increase (respectively decrease) of the reflection coefficient (respectively transmission coefficient) is observed both analytically and numerically around $W/h = 1$, especially for high roughness and high frequencies. However, for higher h and for higher f_c, significant differences are obtained between analytical and numerical results. In particular, for $h = 40$ µm and $f_c = 10$ and

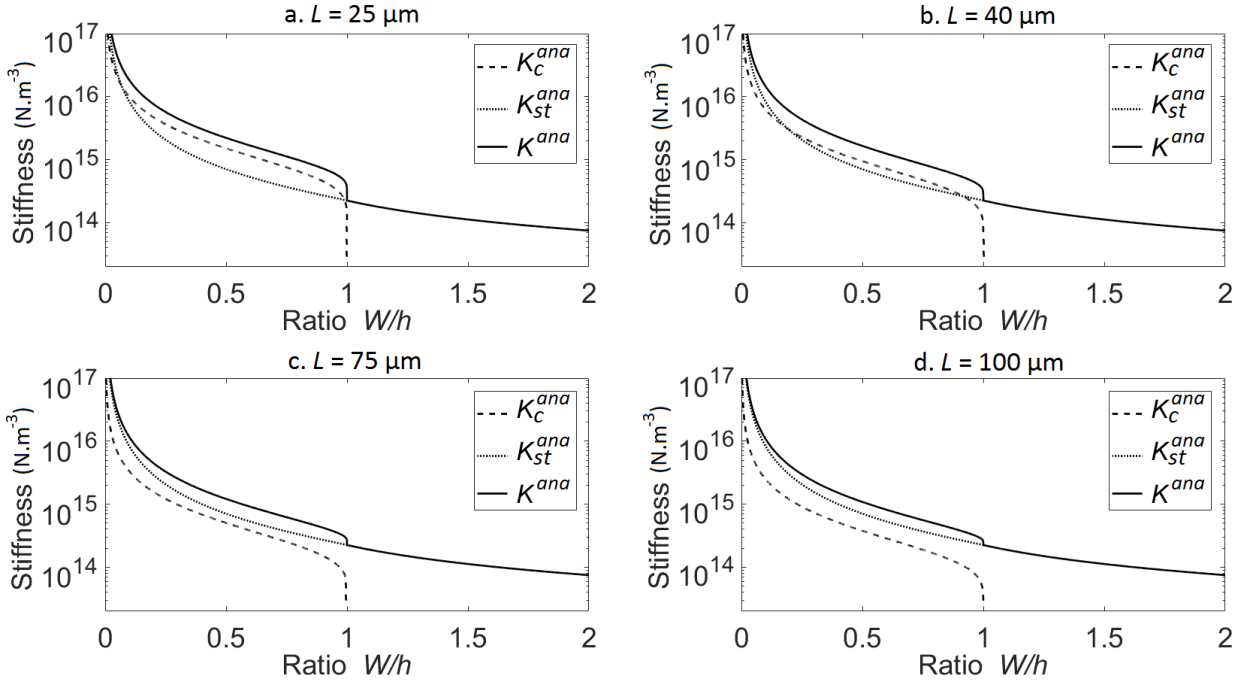

Figure 7: Variation of the analytical total stiffness of the BII K^{ana} and of the stiffness contributions K_c^{ana} and K_{st}^{ana} corresponding to the bone-implant contact and to soft tissues, respectively, as a function of the ratio of the soft tissues thickness W and the roughness amplitude h for h = 20 µm and (a) L = 25 µm, (b) L = 40 µm, (c) $L = 75\ \mu m$, (d) L = 100 µm

15 MHz, (i) for $W/h < 0.25$, the values of r^{num} are significantly lower than values of r^{ana} and (ii) for $W/h > 1.5$, r^{num} (respectively t^{num}) reaches a constant value, while r^{ana} (respectively t^{ana}) still increases (respectively decreases) as a function of W/h.

Figure 10 shows the evolution of the error e_1 between analytical and numerical results and of the error e_2 corresponding to the difference between r^{static} and r^{num} as a function of h for L = 50 µm. Both error functions increase as a function of h. Furthermore, while considering numerical stiffness values K^{num} leads to lower errors than considering analytical stiffness values K^{ana}, the error difference between the two approaches remains relatively low (around 2.5×10^{-3}). For all the configurations tested, the error between analytical and numerical models remained lower than 2.6×10^{-2}.

4. Discussion

4.1. Originality and comparison with the literature

The originality of this work is to provide an analytical model describing the interaction between an ultrasonic wave and the BII. The proposed model was validated through a comparison with numerical results obtained with FEM studies. Moreover, while most studies in the literature dealing with ultrasonic propagation at rough interfaces were performed in the frequency domain [3, 21, 42, 43], the present study was performed in the time domain, which is closer to configurations of interest.

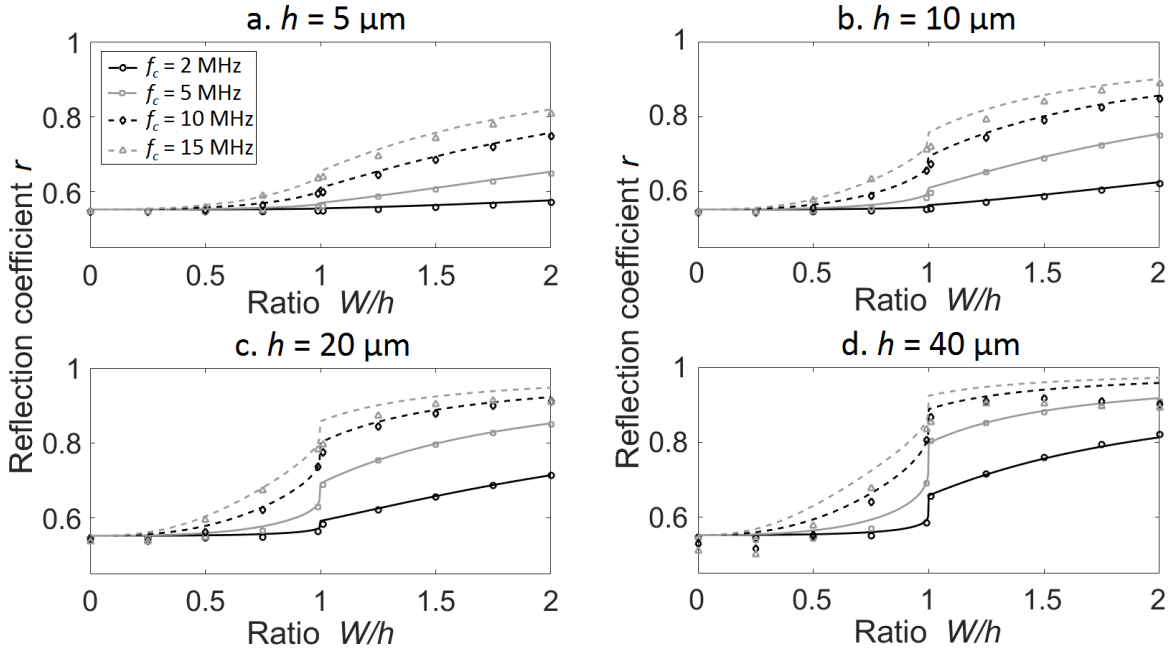

Figure 8: Variation of the reflection coefficient of the BII as a function of the ratio of the soft tissues thickness W and the roughness amplitude h for $L = 50$ µm, for different frequencies f_c and for (a) $h = 5$ µm, (b) $h = 10$ µm, (c) $h = 20$ µm, (d) $h = 40$ µm. Solid lines represent the analytical values r^{ana} whereas the symbols represent the numerical values r^{num}.

The present work is related to the studies performed in Heriveaux et al. [18, 17]. In particular, the numerical model and the sinusoidal description of the BII considered herein were taken from these previous studies. Given the equivalence between profilometry-measured implant profiles and sinusoidal profiles established in Heriveaux et al. [17], the analytical model described herein could be generalized to real implant surface profiles. However, the macroscopic roughness of implants (*e.g.* threading of dental implants) was not considered in the present study because it would lead to interference phenomena [18], which could not be taken into account with a 2-D analytical model. In particular, Heriveaux et al. [18] evidenced significant interferences of the echoes from summits and valleys of the rough interface, and multiple scattering phenomena.

Similarly as in Dwyer-Joyce et al. [7], the present study separately assessed the stiffness contributions due to liquid and solid contact in order to determine the equivalent stiffness of a rough interface. In this former study, a lubricant layer was confined at the interface, while soft tissues were considered between the bone and the implant in the present study. In both studies, the analytical spring model was validated through comparisons with experimental or numerical results. However, lubrication aims at impeding the direct contact of surfaces, so that the contact stiffness contribution always remained lower than the lubricant layer contribution in Dwyer-Joyce et al. [7], which is a different situation compared to the present study. At the beginning of the osseointegration process ($W \geq 0.8\ h$), the BIC ratio is relatively low, so that K_c is low compared to K_{st}. However, at the end of the osseointegration process ($W = 0$) the bone and the implant are in intimate contact, so that K_c may be higher than K_{st}. Therefore, both K_c and K_{st} may be predominant herein depending on the configuration of the BII (see Fig. 6 and 7). Different models of contact stiffness [23, 22] had thus to be considered in the present study and in Dwyer-Joyce

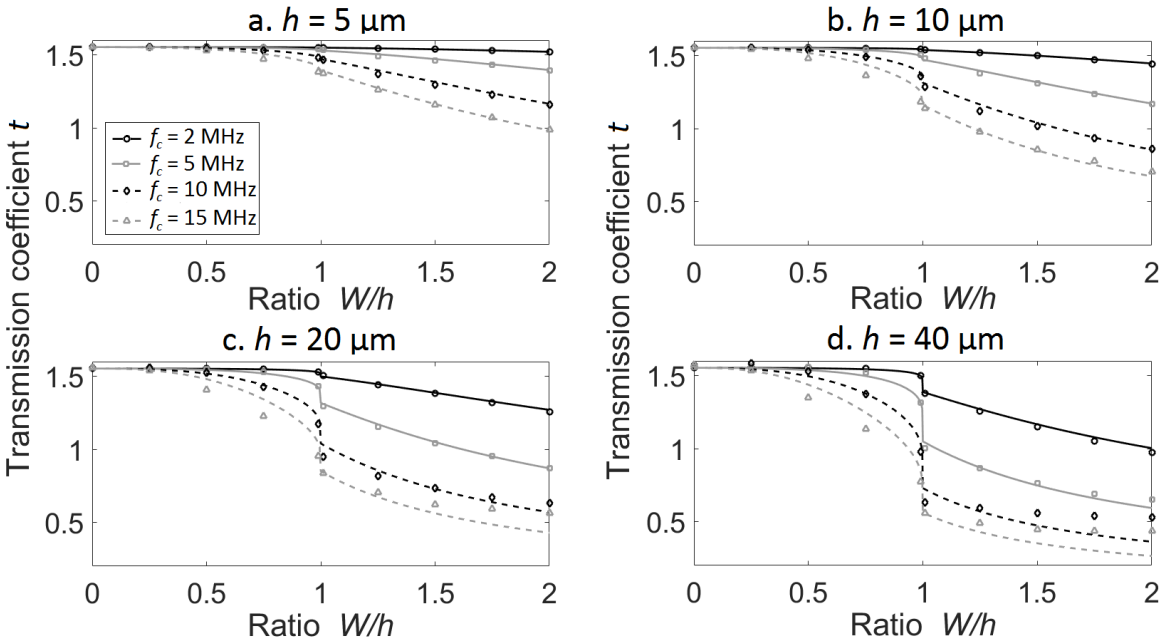

Figure 9: Variation of the transmission coefficient of the BII as a function of the ratio of the soft tissues thickness W and the roughness amplitude h for $L = 50$ µm, for different frequencies f_c and for (a) $h = 5$ µm, (b) $h = 10$ µm, (c) $h = 20$ µm, (d) $h = 40$ µm. Solid lines represent the analytical values t^{ana} whereas the symbols represent the numerical values t^{num}.

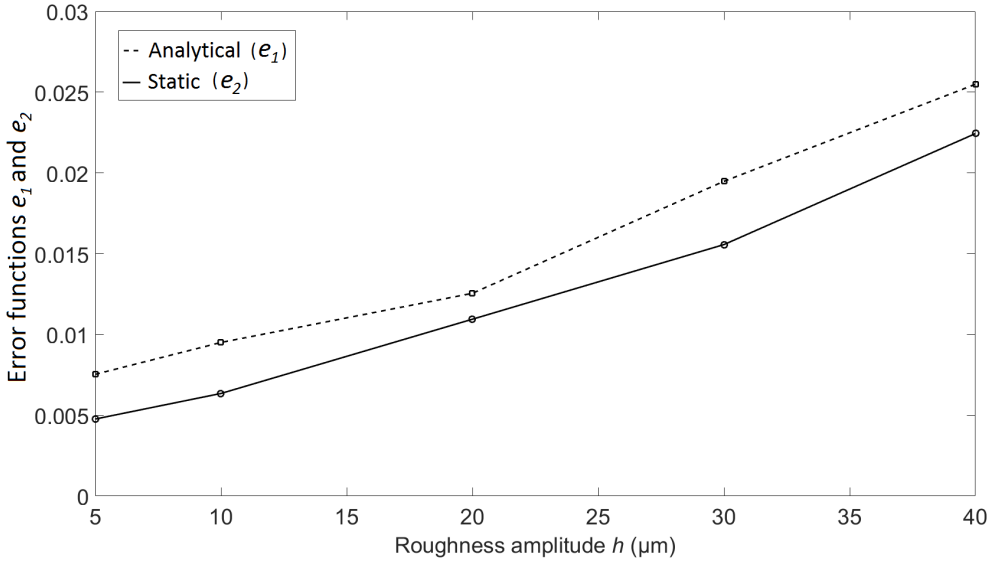

Figure 10: Evolution of the error functions e_1 and e_2 as a function of the the roughness amplitude h for $L = 50$ µm

et al. [7]. Moreover, the loss of validity of the analytical formula of K_{st}^{ana} for low values of W (see Fig. 5) may be due to the fact that this formulation was designed for a configuration with low contact area at the interface ($K_c < K_{st}$).

Figure 8 showed that the reflection coefficient increases as a function of W, which may be

explained by the increase of the gap of acoustical properties when soft tissues are in contact with the implant surface compared to a fully bonded interface. This result is in qualitative agreement with previous experimental [28, 53, 51] and numerical studies [49, 50]. Note that it is also possible to change the properties of bone tissue in the analytical model (see Eq. 14) in order to take into account the evolution of the biomechanical properties of bone, similarly to what was done in Heriveaux et al. [18]. In particular, Heriveaux et al. [18] investigated the influence on r^{num} of a decrease of the bone mass density ρ by 20% compared to its reference value ρ_0. Table 3 shows the values of r^{num} and r^{ana} obtained for $\rho = \rho_0$ and for $\rho = 0.8\ \rho_0$ for a given configuration ($h = 5$ µm; $L = 50$ µm; $W = h/2$ and $f_c = 10$ MHz). The low difference between r^{num} and r^{ana} when decreasing ρ by 20% further validates the analytical model.

Table 3: Values of the numerical and analytical reflection coefficients r^{num} and r^{ana} obtained considering a bone mass density ρ equal to its reference value ρ_0 or to 80% of ρ_0. Other parameters were set to the following values : h = 5 µm; L = 50 µm; $W = h/2$ and f_c = 10 MHz

	r^{num}	r^{ana}
$\rho = \rho_0$	0.5508	0.5575
$\rho = 0.8\ \rho_0$	0.6215	0.6280

4.2. Error between analytical and numerical results

Figures 8 and 9 show that analytical reflection and transmission coefficients (r^{ana}, t^{ana}) are in good agreement with numerical results. However, the error e_1 between analytical and numerical models was only estimated based on values of r^{ana} and not of t^{ana} because the reflection coefficient is the parameter of interest when investigating the properties of the BII with QUS [28, 53, 51, 20]. In particular, e_1 could be compared with the experimental precision $P = 0.011$ on the estimation of the reflection coefficient assessed in Mathieu et al. [28]. For roughness amplitudes h lower than 20 µm, the error between analytical and numerical models remains lower to the experimental error (see Fig. 10). Consequently, for standard values of implant roughness, the analytical modeling of the BII should be sufficient to derive an accurate description of its ultrasonic response.

Moreover, Figs. 4 and 5 show that there are some differences between the values of K^{num} and K^{ana}, especially for low values of W and high values of h. In particular, the loss of validity of the analytical formula of K_{ana} for higher values of h may be due to the fact that the model from Lekesiz et al. [23] assumes an interface with flat cracks with vanishing volume. However, e_1 and e_2, which represent the error between r^{num} and r^{ana} and the error between r^{num} and r^{static}, respectively, are within the same order of magnitude. Therefore, the errors between K^{ana} and K^{num} have a relatively weak influence on the estimation of the reflection coefficient. It may be explained as follows. Equation 14 shows that the evolution of r^{ana} is especially sensitive to K when it has values around $(Z_{ti}Z_b\omega)/(Z_{ti} + Z_b)$, which corresponds to $K = 7.2 \times 10^{13}$ N/m^3 at 2 MHz, and $K = 5.4 \times 10^{14}$ N/m^3 at 15 MHz. However, errors between K^{ana} and K^{num} are most significant for stiffness values superior to 5×10^{14} N/m^3, which therefore weakly affect the reflection coefficient. Furthermore, the higher sensitivity of r^{ana} and t^{ana} to values of K around $(Z_{ti}Z_b\omega)/(Z_{ti} + Z_b)$ also explains that the errors between the analytical and numerical models are lower for lower frequencies (see Fig. 8 and 9).

4.3. Contributions of K_c and K_{st}

Figures 6 and 7 show that the contribution of the contact stiffness K_c is predominant compared to the one soft tissues when the implant roughness is high, *i.e.* for high values of h and for low values of L. It may be due to the fact that a higher implant roughness leads to a higher contact area between the bone and the implant, and therefore to an increase of K_c. Moreover, for higher roughness, a steeper increase (respectively decrease) of r^{ana} and r^{num} (respectively of t^{ana} and t^{num}) is observed around $W = h$. It may be explained as follows. Since K_c is predominant compared to K_{st} for higher roughness, the sudden decrease of K_c when W approaches h has a higher influence on the ultrasonic propagation at the BII in that configuration. Moreover, the steep increase of r around $W = h$ also depends on the frequency since r is especially sensitive to K for a given range of values which depends on the frequency, as described in last section.

4.4. Limitations

This study has several limitations. First, the flat spring-interface model used for the analytical model is a strong approximation that may not take into account interference phenomena, which are known to occur for high implant roughness [18]. In particular, reflection coefficients cannot be lower than 0.55 using the analytical model (which corresponds to $(Z_{ti} - Z_b)/(Z_{ti} + Z_b)$, see Eq. 14), while numerical results showed lower reflection coefficients for high roughness (see Eq. 14). The error between numerical and analytical results may also be related to the geometrical approximation of the BII by an array of periodic cracks to assess analytical contact stiffness (see Section 2.3.1), which may lose in validity for higher roughness. In particular, it may explain that the difference between K_c^{ana} and K_c^{num} (respectively between K_{st}^{ana} and K_{st}^{num}) increased as a function of h in Fig. 4 (respectively in Fig. 5).

Second, only the direction of propagation from the implant to the bone tissue was taken into account because it corresponds to the experimental situation of interest [28, 53, 51]. Future studies should account for oblique incidences.

Third, the variation of the periprosthetic bone geometrical properties is rather simple and modeled by a bone level given by the parameter W, while the bone geometry around the implant surface is likely to be much more complex.

Fourth, the sinusoidal description of the implant surface profile is a strong approximation. However, this approach was validated in Heriveaux et al. [17] through a comparison with ultrasonic responses of real implant surface profiles measured by profilometry.

Fifth, bone materials properties were assumed to be elastic, homogeneous and isotropic, similarly as what was done in some previous studies [25, 49, 50]. However, bone tissue is known to be a strongly dispersive medium [12, 14], which was neglected herein. Moreover, although mature bone tissue is known to be anisotropic [11, 40], the anisotropic behavior of newly formed bone tissue remains unknown [26, 45]. In future works, the heterogeneity of bone tissue could be considered using the approach of Argatov and Iantchenko [2], that developed an acoustical model in the case of continuously stratified tissues.

Sixth, adhesion phenomena at the BII [28], which may lead to a non-linear ultrasonic response [4] were not taken into account in the present study.

5. Conclusion

This study provides an analytical model of the ultrasonic propagation at the BII. The proposed model allows to replace the rough and multiphasic BII by a simple bi-spring model but still provides

a good prediction of the reflected and transmitted coefficient measured from time-domain signals. The use of this analytical model may save computation costs for future numerical studies, which can be complex due to the multiscale nature of the interaction between an ultrasonic wave and the BII. However, the analytical model was validated considering an ultrasonic wave in normal incidence. Therefore, it should be carefully used when modeling real implant geometries, in which multiple reflections and thus oblique incidence of the ultrasonic wave on the BII should be considered.

Acknowledgements

This project has received funding from the European Research Council (ERC) under the European Union's Horizon 2020 research and innovation program (grant agreement No 682001, project ERC Consolidator Grant 2015 BoneImplant).

The authors declare no competing interests.

References

[1] de Almeida, M.S., Maciel, C.D., Pereira, J.C., 2007. Proposal for an ultrasonic tool to monitor the osseointegration of dental implants. Sensors (Basel) 7, 1224–37.

[2] Argatov, I., Iantchenko, A., 2013. Resonance spectrum for a continuously stratified layer: Application to ultrasonic testing. Waves in Random and Complex Media 23. doi:10.1080/17455030.2013.768780.

[3] Baik, J.M., Thompson, R.B., 1984. Ultrasonic scattering from imperfect interfaces: A quasi-static model. Journal of Nondestructive Evaluation 4, 177–196. doi:10.1007/bf00566223.

[4] Biwa, S., Nakajima, S., Ohno, N., 2004. On the acoustic nonlinearity of solid-solid contact with pressure-dependent interface stiffness. Journal of Applied Mechanics 71, 508–515. doi:10.1115/1.1767169.

[5] Chung, J., Hulbert, G.M., 1993. A Time Integration Algorithm for Structural Dynamics With Improved Numerical Dissipation: The Generalized-α Method. Journal of Applied Mechanics 60, 371–375. doi:10.1115/1.2900803.

[6] Dundurs, J., 1967. Effect of elastic constants on stress in a composite under plane deformation. Journal of Composite Materials 1, 310–322. doi:10.1177/002199836700100306.

[7] Dwyer-Joyce, R., Reddyhoff, T., Zhu, J., 2011. Ultrasonic measurement for film thickness and solid contact in elastohydrodynamic lubrication. Journal of Tribology 133. doi:10.1115/1.4004105.

[8] Egan, J.M., Marsden, D.C., 2001. A spring network model for the analysis of load transfer and tissue reactions in intra-medullary fixation. Clin Biomech (Bristol, Avon) 16, 71–9. doi:10.1016/s0268-0033(00)00070-x.

[9] England, A.H., 1965. A Crack Between Dissimilar Media. Journal of Applied Mechanics 32, 400–402. doi:10.1115/1.3625813.

[10] Franchi, M., Bacchelli, B., Giavaresi, G., De Pasquale, V., Martini, D., Fini, M., Giardino, R., Ruggeri, A., 2007. Influence of different implant surfaces on peri-implant osteogenesis: Histomorphometric analysis in sheep. Journal of Periodontology 78, 879–888. doi:10.1902/jop.2007.060280.

[11] Haïat, G., Naili, S., Grimal, Q., Talmant, M., Desceliers, C., Soize, C., 2009. Influence of a gradient of material properties on ultrasonic wave propagation in cortical bone: Application to axial transmission. The Journal of the Acoustical Society of America 125, 4043–4052. doi:10.1121/1.3117445.

[12] Haïat, G., Padilla, F., Peyrin, F., Laugier, P., 2008. Fast wave propagation in trabecular bone: numerical study of the influence of porosity and structural anisotropy. Journal of the Acoustical Society of America 123, 1694–1705.

[13] Haïat, G., Wang, H.L., Brunski, J., 2014. Effects of biomechanical properties of the bone–implant interface on dental implant stability: From in silico approaches to the patient's mouth. Annual Review of Biomedical Engineering 16, 187–213. doi:10.1146/annurev-bioeng-071813-104854.

[14] Haiat, G., Naili, S., 2011. Independent scattering model and velocity dispersion in trabecular bone: comparison with a multiple scattering model. Biomechanics and Modeling in Mechanobiology 10, 95–108. doi:10.1007/s10237-010-0220-z.

[15] Haiat, G., Padilla, F., Peyrin, F., Laugier, P., 2007. Variation of ultrasonic parameters with microstructure and material properties of trabecular bone: A 3d model simulation. J Bone Miner Res 22, 665–674. doi:10.1359/jbmr.070209.

[16] Heller, A.L., Heller, R.L., 1996. Clinical evaluations of a porous-surfaced endosseous implant system. J Oral Implantol 22, 240–6.
[17] Heriveaux, Y., Nguyen, V.H., Brailovski, V., Gorny, C., Haiat, G., 2019. Reflection of an ultrasonic wave on the bone-implant interface: effect of the roughness parameters. J Acoust Soc Am 145, 3370–3381.
[18] Heriveaux, Y., Nguyen, V.H., Haiat, G., 2018. Reflection of an ultrasonic wave on the bone-implant interface: A numerical study of the effect of the multiscale roughness. J Acoust Soc Am 144, 488–499. doi:10.1121/1.5046524.
[19] Hériveaux, Y., Haïat, G., Nguyen, V.H., 2020. Reflection of an ultrasonic wave on the bone-implant interface: Comparison of two-dimensional and three-dimensional numerical models. The Journal of the Acoustical Society of America 147, EL32–EL36. doi:10.1121/10.0000500.
[20] Hériveaux, Y., Nguyen, V.H., Geiger, D., Haïat, G., 2019. Elastography of the bone-implant interface. Scientific Reports 9, 14163. doi:10.1038/s41598-019-50665-4.
[21] Jhang, K.Y., 2009. Nonlinear ultrasonic techniques for nondestructive assessment of micro damage in material: A review. International Journal of Precision Engineering and Manufacturing 10, 123–135. doi:10.1007/s12541-009-0019-y.
[22] Królikowski, J., Szczepek, J., Witczak, Z., 1989. Ultrasonic investigation of contact between solids under high hydrostatic pressure. Ultrasonics 27, 45 – 49. doi:https://doi.org/10.1016/0041-624X(89)90008-5.
[23] Lekesiz, H., Katsube, N., Rokhlin, S.I., Seghi, R.R., 2011. Effective spring stiffness for a planar periodic array of collinear cracks at an interface between two dissimilar isotropic materials. Mech Mater 43, 87–98. doi:10.1016/j.mechmat.2010.12.004.
[24] Mathieu, V., Anagnostou, F., Soffer, E., Haïat, G., 2011a. Ultrasonic evaluation of dental implant biomechanical stability: An in vitro study. Ultrasound in Medicine & Biology 37, 262–270. doi:https://doi.org/10.1016/j.ultrasmedbio.2010.10.008.
[25] Mathieu, V., Anagnostou, F., Soffer, E., Haiat, G., 2011b. Numerical simulation of ultrasonic wave propagation for the evaluation of dental implant biomechanical stability. J. Acoust. Soc. Am. 129, 4062–72. doi:10.1121/1.3586788].
[26] Mathieu, V., Fukui, K., Matsukawa, M., Kawabe, M., Vayron, R., Soffer, E., Anagnostou, F., Haiat, G., 2011c. Micro-brillouin scattering measurements in mature and newly formed bone tissue surrounding an implant. J Biomech Eng 133, 021006. doi:10.1115/1.4003131.
[27] Mathieu, V., Vayron, R., Richard, G., Lambert, G., Naili, S., Meningaud, J.P., Haiat, G., 2014. Biomechanical determinants of the stability of dental implants: influence of the bone-implant interface properties. J Biomech 47, 3–13. doi:10.1016/j.jbiomech.2013.09.021.
[28] Mathieu, V., Vayron, R., Soffer, E., Anagnostou, F., Haiat, G., 2012. Influence of healing time on the ultrasonic response of the bone-implant interface. Ultrasound Med Biol 38, 611–8. doi:10.1016/j.ultrasmedbio.2011.12.014.
[29] Meredith, N., Alleyne, D., Cawley, P., 1996. Quantitative determination of the stability of the implant-tissue interface using resonance frequency analysis. Clin Oral Implants Res 7, 261–7.
[30] Michel, A., Bosc, R., Meningaud, J.P., Hernigou, P., Haiat, G., 2016. Assessing the acetabular cup implant primary stability by impact analyses: A cadaveric study. PLoS One 11, e0166778. doi:10.1371/journal.pone.0166778.
[31] Moerman, A., Zadpoor, A.A., Oostlander, A., Schoeman, M., Rahnamay Moshtagh, P., Pouran, B., Valstar, E., 2016. Structural and mechanical characterisation of the peri-prosthetic tissue surrounding loosened hip prostheses. an explorative study. J Mech Behav Biomed Mater 62, 456–467. doi:10.1016/j.jmbbm.2016.04.009.
[32] Njeh, C.F., Hans, D., Wu, C., Kantorovich, E., Sister, M., Fuerst, T., Genant, H.K., 1999. An in vitro investigation of the dependence on sample thickness of the speed of sound along the specimen. Medical Engineering & Physics 21, 651–659. doi:https://doi.org/10.1016/S1350-4533(99)00090-9.
[33] Pastrav, L.C., Jaecques, S.V., Jonkers, I., Perre, G.V., Mulier, M., 2009. In vivo evaluation of a vibration analysis technique for the per-operative monitoring of the fixation of hip prostheses. J Orthop Surg Res 4, 10. doi:10.1186/1749-799x-4-10.
[34] Pattijn, V., Jaecques, S.V.N., De Smet, E., Muraru, L., Van Lierde, C., Van der Perre, G., Naert, I., Vander Sloten, J., 2007. Resonance frequency analysis of implants in the guinea pig model: Influence of boundary conditions and orientation of the transducer. Medical Engineering & Physics 29, 182–190. doi:https://doi.org/10.1016/j.medengphy.2006.02.010.
[35] Pattijn, V., Van Lierde, C., Van der Perre, G., Naert, I., Vander Sloten, J., 2006. The resonance frequencies and mode shapes of dental implants: Rigid body behaviour versus bending behaviour. a numerical approach. Journal of Biomechanics 39, 939–947. doi:https://doi.org/10.1016/j.jbiomech.2005.01.035.

[36] Pecorari, C., Poznic, M., 2006. On the linear and nonlinear acoustic properties of dry and water-confining elasto-plastic interfaces. Proceedings of the Royal Society A: Mathematical, Physical and Engineering Sciences 462, 769–788. doi:10.1098/rspa.2005.1595.

[37] Pilliar, R.M., Lee, J.M., Maniatopoulos, C., 1986. Observations on the effect of movement on bone ingrowth into porous-surfaced implants. Clin Orthop Relat Res 208, 108–13.

[38] Raffa, M.L., Nguyen, V.H., Haiat, G., 2019. Micromechanical modeling of the contact stiffness of an osseointegrated bone–implant interface. BioMedical Engineering OnLine 18, 114. doi:10.1186/s12938-019-0733-3.

[39] Rittel, D., Dorogoy, A., Haiat, G., Shemtov-Yona, K., 2019. Resonant frequency analysis of dental implants. Med Eng Phys 66, 65–74.

[40] Sansalone, V., Bousson, V., Naili, S., Bergot, C., Peyrin, F., Laredo, J.D., Haïat, G., 2012. Anatomical distribution of the degree of mineralization of bone tissue in human femoral neck: Impact on biomechanical properties. Bone 50, 876–884. doi:https://doi.org/10.1016/j.bone.2011.12.020.

[41] Schulte, W., d'Hoedt, B., Lukas, D., Muhlbradt, L., Scholz, F., Bretschi, J., Frey, D., Gudat, H., Konig, M., Markl, M., et al., 1983. [periotest–a new measurement process for periodontal function]. Zahnarztl Mitt 73, 1229–30, 1233–6, 1239–40.

[42] Tattersall, H.G., 1973. The ultrasonic pulse-echo technique as applied to adhesion testing. Journal of Physics D: Applied Physics 6, 819–832. doi:10.1088/0022-3727/6/7/305.

[43] Thompson, D.O., Chimenti, D.E., 2011. Review of Progress in Quantitative Nondestructive Evaluation: Volume 30A. American Institute of Physics; 2011 edition.

[44] Tijou, A., Rosi, G., Vayron, R., Lomami, H.A., Hernigou, P., Flouzat-Lachaniette, C.H., Haïat, G., 2018. Monitoring cementless femoral stem insertion by impact analyses: An in vitro study. Journal of the Mechanical Behavior of Biomedical Materials 88, 102–108. doi:https://doi.org/10.1016/j.jmbbm.2018.08.009.

[45] Vayron, R., Barthel, E., Mathieu, V., Soffer, E., Anagnostou, F., Haiat, G., 2012. Nanoindentation measurements of biomechanical properties in mature and newly formed bone tissue surrounding an implant. Journal of Biomechanical Engineering 134, 021007–021007–6. doi:10.1115/1.4005981.

[46] Vayron, R., Karasinski, P., Mathieu, V., Michel, A., Loriot, D., Richard, G., Lambert, G., Haiat, G., 2013. Variation of the ultrasonic response of a dental implant embedded in tricalcium silicate-based cement under cyclic loading. Journal of Biomechanics 46, 1162–1168. doi:https://doi.org/10.1016/j.jbiomech.2013.01.003.

[47] Vayron, R., Mathieu, V., Michel, A., Haïat, G., 2014a. Assessment of in vitro dental implant primary stability using an ultrasonic method. Ultrasound in Medicine & Biology 40, 2885–2894. doi:https://doi.org/10.1016/j.ultrasmedbio.2014.03.035.

[48] Vayron, R., Matsukawa, M., Tsubota, R., Mathieu, V., Barthel, E., Haiat, G., 2014b. Evolution of bone biomechanical properties at the micrometer scale around titanium implant as a function of healing time. Physics in medicine and biology 59, 1389–1406.

[49] Vayron, R., Nguyen, V.H., Bosc, R., Naili, S., Haïat, G., 2015. Finite element simulation of ultrasonic wave propagation in a dental implant for biomechanical stability assessment. Biomech Model Mechanobiol 14, 1021–32. doi:10.1007/s10237-015-0651-7.

[50] Vayron, R., Nguyen, V.H., Bosc, R., Naili, S., Haïat, G., 2016. Assessment of the biomechanical stability of a dental implant with quantitative ultrasound: A three-dimensional finite element study. The Journal of the Acoustical Society of America 139, 773–780. doi:10.1121/1.4941452.

[51] Vayron, R., Nguyen, V.H., Lecuelle, B., Albini Lomami, H., Meningaud, J.P., Bosc, R., Haiat, G., 2018a. Comparison of resonance frequency analysis and of quantitative ultrasound to assess dental implant osseointegration. Sensors (Basel, Switzerland) 18, 1397. doi:10.3390/s18051397.

[52] Vayron, R., Nguyen, V.H., Lecuelle, B., Haiat, G., 2018b. Evaluation of dental implant stability in bone phantoms: Comparison between a quantitative ultrasound technique and resonance frequency analysis. Clin Implant Dent Relat Res doi:10.1111/cid.12622.

[53] Vayron, R., Soffer, E., Anagnostou, F., Haïat, G., 2014c. Ultrasonic evaluation of dental implant osseointegration. Journal of Biomechanics 47, 3562–3568. doi:https://doi.org/10.1016/j.jbiomech.2014.07.011.